CrystEngComm

COMMUNICATION

View Article Online
View Journal | View Issue

Cite this: *CrystEngComm*, 2015, **17**, 4774

Received 31st March 2015,
Accepted 22nd May 2015

DOI: 10.1039/c5ce00635j

www.rsc.org/crystengcomm

Template-free synthesis of β-$Na_{0.33}V_2O_5$ microspheres as cathode materials for lithium-ion batteries

Qinguang Tan,†[a] Qinyu Zhu,†[a] Anqiang Pan,*[a] Yaping Wang,[a] Yan Tang,[a] Xiaoping Tan,[a] Shuquan Liang*[a] and Guozhong Cao*[b]

In this work, hierarchical three-dimensional (3D) β-$Na_{0.33}V_2O_5$ microspheres have been synthesized for the first time by a simple solvothermal reaction with subsequent annealing treatment. The hierarchical microspheres are self-assembled from nanosheet subunits during the solvothermal process. Simultaneously, various hierarchical microspheres with different subunits can be produced by altering the solvothermal solution. After annealing in air, the solvothermal product can be converted into β-$Na_{0.33}V_2O_5$ with a well-retained structure. As cathode materials for lithium ion batteries, the as-prepared 3D microspheres exhibit high capacity and good rate capability. The superior electrochemical performance is attributed to the unique three-dimensional hierarchical microstructures, which mimic the advantages of nano- and microstructures.

1 Introduction

Recently, three-dimensional (3D) nanostructured materials have attracted considerable attention due to their superior physical and chemical properties.[1–5] In particular, they are broadly studied as electrodes for lithium ion batteries (LIBs) because of their capability to maintain the structural integrity, high packing density and good lithium storage properties.[6–9] Moreover, the characteristic hierarchical structures are believed to have better abilities to suppress agglomeration, facilitate electrolyte penetration and accommodate the volume change upon cycling.[10–12] The nanosized building blocks could also effectively reduce the lithium diffusion distance, which could significantly improve the rate capability and capacity retention.[10,13,14] To date, the hierarchical micro/nanostructures, such as porous frameworks,[1,15–18] hollow structured microspheres[13,19] and urchin-like microflowers,[20,21] have been fabricated to investigate their electrochemical properties. However, the majority of reports are based on metal oxides with simple compositions. It is still a big challenge to fabricate hierarchical lithium/sodium transition metal oxides with complex compositions, such as $LiMn_2O_4$ and $Na_{0.33}V_2O_5$, which significantly limits their applications.[22–29]

Vanadium oxides and their derivatives have attracted research interest as alternative cathode materials for LIBs for decades, mainly because of their high specific capacities, low cost and abundant resources.[16,29–37] Among the vanadium oxide derivatives, β-phase $Na_{0.33}V_2O_5$ is believed to be a promising candidate due to its 3D tunneled crystal structure and high capacity.[38–41] To date, low dimensional β-$Na_{0.33}V_2O_5$ nanowires[42,43] and mesoporous nanoflakes[39] have been reported to have improved electrochemical performance. However, the synthesis of β-$Na_{0.33}V_2O_5$ hierarchical structures is rarely reported.

Herein, we report the fabrication of β-$Na_{0.33}V_2O_5$ hierarchical microspheres by a solvothermal approach with a subsequent annealing process in air. The solvothermally prepared microspheres are assembled from small nanosheets and the structures can be safely retained after calcination in air. As cathode materials for lithium ion batteries, the β-$Na_{0.33}V_2O_5$ microspheres exhibit high capacity and good rate capability.

2 Experimental section

Materials preparation

V_2O_5 (0.36 g) and $H_2C_2O_4{\cdot}2H_2O$ in a molar ratio of 1 : 3 were dissolved in 12 mL of distilled water under vigorous stirring at 60 °C for several hours until a clear blue solution was formed. Then, $NaHCO_3$ with different molar ratios (Na : V = 1 : 4, 1 : 6 and 1 : 3) was separately added to the above-prepared solution under stirring for 20 minutes. After that, 60 mL of isobutanol was added to prepare the mixture

[a] *School of Materials Science & Engineering, Central South University, Changsha, Hunan, 410083, China. E-mail: pananqiang@csu.edu.cn, lsq@mail.csu.edu.cn*
[b] *Department of Materials Science & Engineering, University of Washington, Seattle, 98195, USA. E-mail: gzcao@u.washington.edu*
† These authors contributed equally to this manuscript.

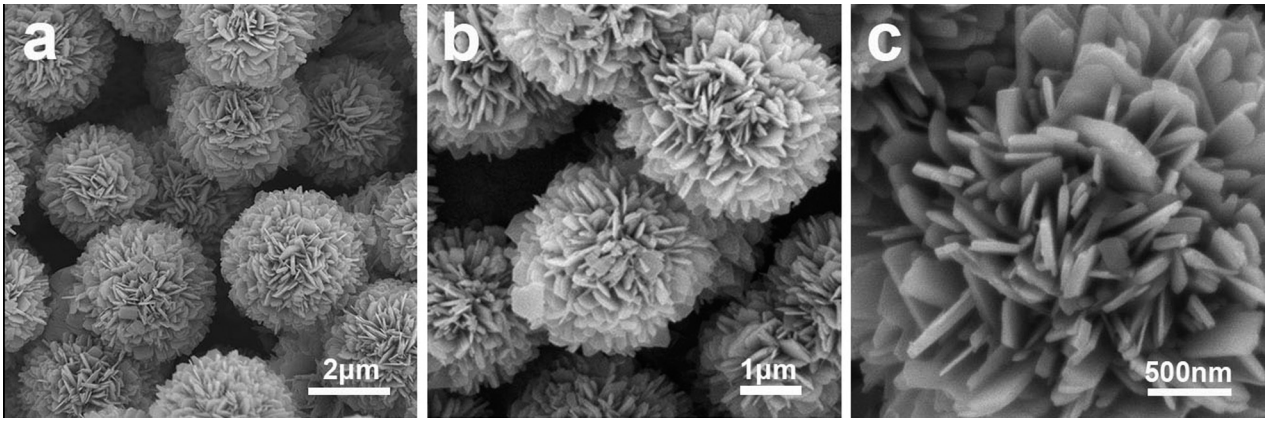

Fig. 1 FESEM images (a, b, c) with different magnifications of the hierarchical microsphere precursor solvothermally prepared at 180 °C for 48 hours (NVO-1 precursor).

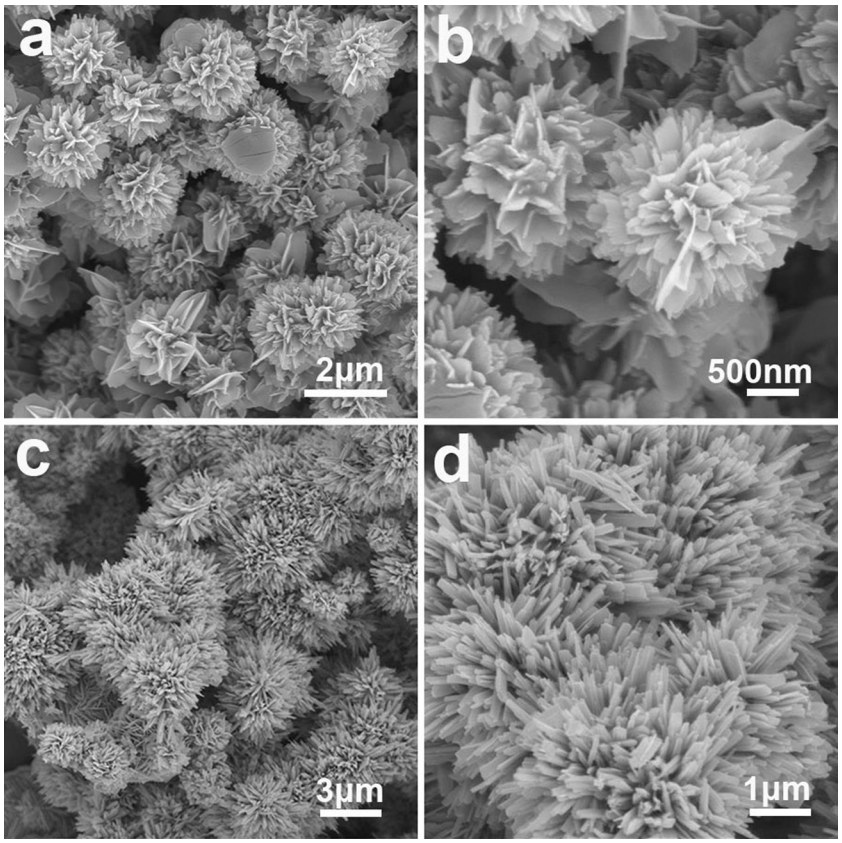

Fig. 2 FESEM images of the hierarchical microflowers solvothermally prepared after changing the amount of $NaHCO_3$: (a and b) NVO-2 precursor; (c and d) NVO-3 precursor.

solution, which was transferred into a sealed 100 mL Teflon container and treated in an electrical oven at 180 °C for 48 h. The obtained precursors were collected by centrifugation and washed twice with pure ethanol, followed by drying at 70 °C overnight. The as-prepared precursors were annealed in air at 400 °C for 3 h with a heating rate of 1 °C min^{-1}. The as-synthesized products obtained with molar ratios of Na : V = 1 : 4, 1 : 6 and 1 : 3 were designated as NVO-1, NVO-2 and NVO-3, respectively.

Materials characterization

TG and DSC analyses were performed on a combined differential scanning calorimetry and thermogravimetric analysis instrument (Netzsch STA 449C, Germany). The crystallographic phases of all the products were investigated by powder X-ray diffraction (XRD, Rigaku D/max 2500) with Cu Kα (λ = 1.5406 Å) radiation. The morphologies of samples were examined by field-emission scanning electron microscopy (SEM, FEI Nova NanoSEM 230) and transmission electron

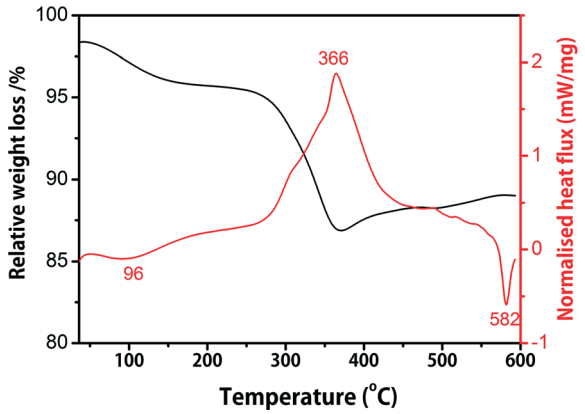

Fig. 3 TG and DSC results of the as-obtained precursor after the solvothermal process. The heating rate was set to 10 °C min^{-1}.

microscopy (TEM, JEOL-JEM-2100F transmission electron microscope).

Electrochemical measurements

The working cathode slurry was prepared by dispersing the β-$Na_{0.33}V_2O_5$, acetylene black and poly(vinylidene fluoride) (PVDF) binder in *N*-methylpyrrolidone solution at a weight ratio of 70 : 20 : 10. The slurry was painted on an aluminum foil and dried in a vacuum oven at 110 °C overnight prior to coin-cell assembly. A lithium foil was used as the current collector and reference electrode, and 1.0 M $LiPF_6$ in ethyl carbonate/dimethyl carbonate (1 : 1 v/v ratio) was used as the electrolyte. Cyclic voltammetry (CV) measurements were performed on an electrochemical workstation (CHI604E, China). The galvanostatic charge/discharge performance of the electrodes was evaluated at room temperature using a Land battery tester (Land CT 2001A, China). Electrochemical impedance spectrometry (EIS) was carried out on a ZAHNER-IM6ex electrochemical workstation in the frequency range of 100 KHz to 10 mHz.

3 Results and discussion

Fig. 1 shows the SEM images of the solvothermally prepared microsphere precursors at different magnifications. As shown in Fig. 1a and b, the solvothermal products obtained with the molar ratio of Na : V = 1 : 4 are of spherical morphology, the diameter of which is about 4 μm. The microspheres are monodispersed. The higher magnification SEM image (Fig. 1c) further reveals the detailed structures of the microspheres, which are assembled from discrete nanosheets with a thickness of about 30 nm. The formation of hierarchical microspheres in the solvothermal process is attributed to the mixed solvent (isobutanol and water). The whole solvent can

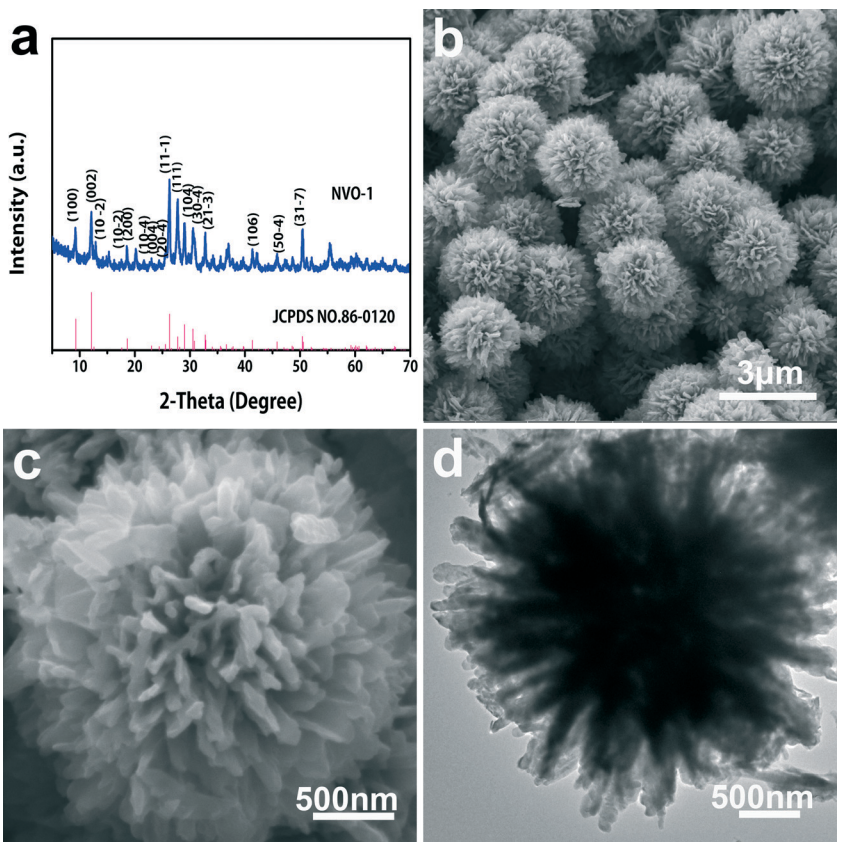

Fig. 4 (a) XRD pattern, (b and c) FESEM images and (d) TEM image of the as-synthesized β-$Na_{0.33}V_2O_5$ microspheres (NVO-1) obtained by annealing the precursor microspheres at 400 °C for 3 h.

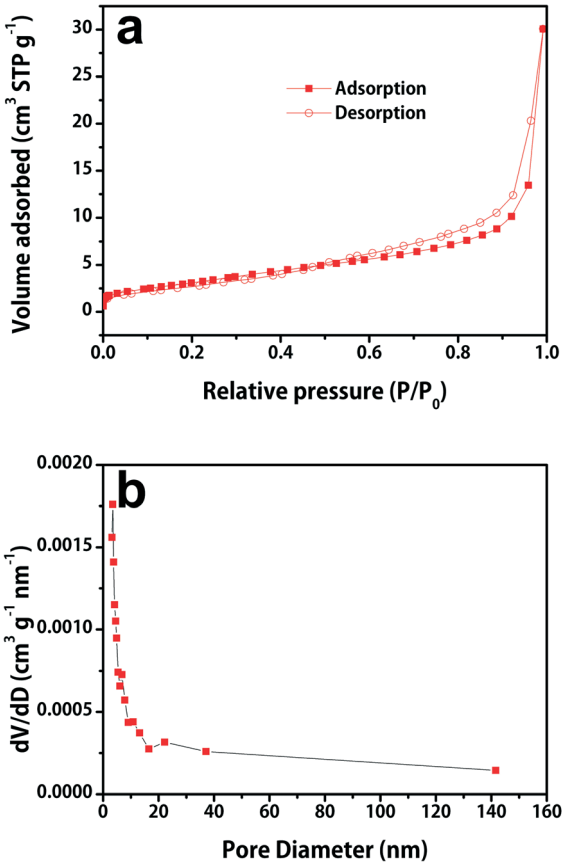

Fig. 5 (a) Nitrogen adsorption–desorption isotherm and (b) the corresponding pore size distribution of the β-$Na_{0.33}V_2O_5$ microspheres.

be considered as the accumulation of small water and isobutanol droplets, and the precursor subunits are formed within these droplets. When the subunits grow big enough, they will break the volume limitation of the small droplets and the subunits will merge together in order to reduce the surface energy to reach a more thermodynamically stable state. Therefore, the hierarchical microspheres will be formed. As shown in Fig. 2a and b, when $NaHCO_3$ with a molar ratio of Na : V = 1 : 6 was added to the solvothermal solution, nanosheet-structured microflowers were obtained after solvothermal treatment. The diameter of the microflowers was much smaller, ranging from 2 to 3 μm. As shown in Fig. 2c and d, urchin-like NVO-3 nano/microstructures could be produced when $NaHCO_3$ with a higher molar ratio of Na : V = 1 : 3 was employed. The urchin-like subunits were composed of nanobelts with a length of about 3 μm. Also, the urchin-like microspheres were the largest among the three solvothermally prepared samples. When a higher amount of $NaHCO_3$ was added, the subunits of the hierarchical microstructures changed from nanosheets to nanobelts. The morphology change may be attributed to the higher concentration of Na^+ ions, which may serve as the nuclei centers of the precursors. When more Na^+ ions are provided in the solvothermal solution, more subunits start to grow and the species in the solution are depleted much faster, thus smaller subunits (nanobelts) are formed. This behavior is a little similar to that in the previous report on the synthesis of VO_2 microstructures.[20] The results demonstrated that hierarchical microstructures with different morphologies can be obtained by simply altering the amount of added $NaHCO_3$.

Fig. 3 shows the TG and DSC results of the precursor microspheres calcined in air using a heating rate of 10 °C min^{-1}. The first weight loss below 250 °C is attributed to the evaporation of the physically absorbed and crystalline hydrate in the precursor. The main weight loss in the TG curve and the corresponding exothermic peak in the DSC curve at 366 °C are ascribed to the formation of β-$Na_{0.33}V_2O_5$. The sharp endothermic peak in the DSC curve at 582 °C suggests the melting of β-$Na_{0.33}V_2O_5$. After annealing in air, the precursor microspheres can be converted into β-$Na_{0.33}V_2O_5$ with well-preserved morphologies. Fig. 4a shows the XRD pattern of the product (NVO-1) calcined in air at a relatively low temperature of 400 °C for 3 h, which can be indexed to a β-$Na_{0.33}V_2O_5$ phase (space group: *A*2/*m* (12), JCPDS card 86-0120).[38,39] A panoramic view of the product (Fig. 4b) demonstrates that the morphologies of the microspheres obtained from the solvothermal products after annealing in air are well preserved. The space between neighboring nanosheets is clearly detected (Fig. 4c). The nanosheet subunits shrunk to smaller nanosheets during the annealing process, which may be attributed to the recrystallization of the precursor when it was converted into β-$Na_{0.33}V_2O_5$. The TEM image (see Fig. 4d) reveals that the microspheres are composed of nanosheet subunits and are of high porosity. The good porosity is beneficial for electrolyte penetration into the electrode materials. The hierarchical nature of the β-$Na_{0.33}V_2O_5$ microspheres is further evaluated by nitrogen adsorption–desorption measurement and the results are shown in Fig. 5. The isothermal curve exhibits a typical χ type, indicating macroporous characteristics. The measured Brunauer–Emmett–Teller (BET) area of the β-$Na_{0.33}V_2O_5$ microspheres is 12.5 m^2 g^{-1}. Barrett–Joyner–Halenda (BJH) calculations disclose that the pore size distribution is in the range of 3–20 nm, which is in good correspondence with the TEM image.

The β-$Na_{0.33}V_2O_5$ microspheres were assembled into coin-cells and evaluated as cathode materials for LIBs. Fig. 6a shows the typical cyclic voltammetry (CV) curve of the β-$Na_{0.33}V_2O_5$ microspheres at a scan rate of 0.1 mV s^{-1} between 1.5 and 4.0 V *vs.* Li/Li^+. During the cathodic scan, five cathodic peaks located at 3.22, 2.88, 2.46, 2.20 and 1.88 V are observed, indicating the multiple-step lithium ion intercalation process.[35–37] Fig. 6b shows both the representative discharge–charge profiles of the β-$Na_{0.33}V_2O_5$ electrode between 1.5 and 4.0 V at current densities of 50, 600 and 1000 mA g^{-1}. The potentials for the five plateaus on the discharge profiles of the first cycle are highly consistent with the CV results. The β-$Na_{0.33}V_2O_5$ microspheres exhibit high initial specific capacities of 249, 216, and 157 mA h g^{-1} at current densities of 50, 600 and 1000 mA g^{-1}, respectively, indicating the good rate capability of the electrode materials. Fig. 6c shows the

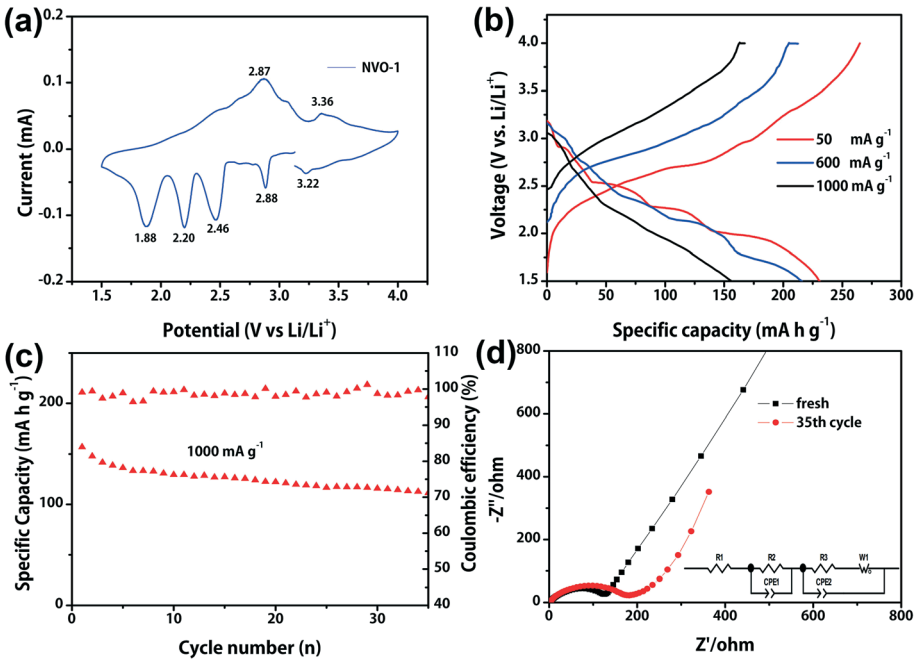

Fig. 6 (a) Typical cyclic voltammogram (CV) curve of the β-$Na_{0.33}V_2O_5$ microspheres at a scan rate of 0.1 mV s^{-1}; (b) discharge–charge profiles of the β-$Na_{0.33}V_2O_5$ microspheres in the first two cycles at current densities of 50, 600 and 1000 mA g^{-1}; (c) cycling performance of the β-$Na_{0.33}V_2O_5$ microspheres in the voltage range of 1.5–4.0 V at a high current density of 1000 mA g^{-1}; (d) Nyquist plots of the β-$Na_{0.33}V_2O_5$ microsphere electrodes in the fresh state and after 35 cycles charged to 4 V.

cycling performance of the β-$Na_{0.33}V_2O_5$ microspheres at a current density of 1000 mA g^{-1}. They exhibit an initial discharge capacity of 157 mA h g^{-1} and retain a specific discharge capacity of 111 mA g^{-1} after 35 cycles. The average capacity fading rate per cycle is 0.8%. The good cycling performance at high current density can be attributed to the novel three dimensional microstructures assembled from nanosheet building blocks. The hierarchical 3D microspheres can limit self-aggregation upon cycling. The large space between neighboring subunits can provide pathways for easy electrolyte penetration and the nanosized subunits can shorten lithium ion diffusion and electron transport distances, thus allowing the electrode to obtain good rate capability and cyclic stability. In order to study the transport kinetics of the electrochemical properties of the microspheres, the typical electrochemical impedance spectra of the electrodes were obtained and the Nyquist plots are shown in Fig. 6d. The impedance spectra consist of a depressed semicircle in the high-frequency region and a straight line in the low-frequency region. The semicircle is assigned to the formation of solid electrolyte interface (SEI) films and contact resistance, and the straight line is associated with the diffusion of Li^+ in the electrode materials. In the equivalent circuit model (inset of Fig. 6d), R_1 consists of the electrolyte resistance and ohmic resistances of cell components. R_2 is the resistance of the SEI films while R_3 is the charge transfer resistance of the electrochemical reaction. The value of R_3 increases with cycling due to the increasing thickness of SEI films and irreversible phase transformation, which is commonly seen as a dominant effect on the capacity fading of vanadium based cathodes.[44,45] As shown in the Nyquist plots, for the fresh electrode, the charge transfer resistance value is 121.6 Ω. When the electrode was evaluated for 35 cycles, the charge transfer resistance increases to 181.3 Ω, indicating a slight increase of charge transfer resistance but a lower increase rate compared with that of the mesoporous β-$Na_{0.33}V_2O_5$ electrode.[39] The small charge-transfer resistance can be attributed to the unique hierarchical structures, which shorten the diffusion pathways and improve the structure stability during the cycling processes. To further investigate the structure stability of β-$Na_{0.33}V_2O_5$ electrodes, the

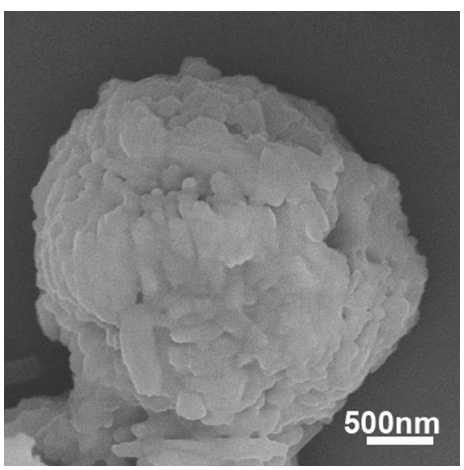

Fig. 7 Morphological analysis of the β-$Na_{0.33}V_2O_5$ microspheres cycled for 35 cycles at a current density of 1000 mA g^{-1}.

morphology of the β-$Na_{0.33}V_2O_5$ microspheres after the cycling processes was characterized by SEM. As shown in Fig. 7, after cycling at 1000 mA g^{-1} for 35 cycles, it is interesting to find that the hierarchical structures of the microspheres can be retained, which indicates the good structural stability of the hierarchical structures.

Conclusions

In summary, 3D hierarchical β-$Na_{0.33}V_2O_5$ microspheres have been successfully synthesized though a simple solvothermal method with a subsequent annealing process. The morphologies of the solvothermally prepared microstructures can be adjusted by changing the amount of added $NaHCO_3$. The nanosheet-assembled microspheres can be converted into β-$Na_{0.33}V_2O_5$ with good structural preservation after annealing. As cathode materials for LIBs, the β-$Na_{0.33}V_2O_5$ microspheres exhibit high rate capability and enhanced cycling stability.

Acknowledgements

This work was supported by the National High-tech R&D Program (863, grant no. 2013AA110106), the National Natural Science Foundation of China (no. 51374255 and 51302323), the Program for New Century Excellent Talents in University (NCET-13-0594), Research Fund for the Doctoral Program of Higher Education of China (no. 201301621200), the Natural Science Foundation of Hunan Province, China (14JJ3018), and the Lie-Ying and Sheng-Hua Program of Central South University.

References

1 Q. An, F. Lv, Q. Liu, C. Han, K. Zhao, J. Sheng, Q. Wei, M. Yan and L. Mai, *Nano Lett.*, 2014, **14**, 6250–6256.
2 J. Bai, X. Li, G. Liu, Y. Qian and S. Xiong, *Adv. Funct. Mater.*, 2014, **24**, 3012–3020.
3 J. S. Chen, D. Luan, C. M. Li, F. Y. Boey, S. Qiao and X. W. Lou, *Chem. Commun.*, 2010, **46**, 8252–8254.
4 X. Fan, J. Shao, X. Xiao, L. Chen, X. Wang, S. Li and H. Ge, *J. Mater. Chem. A*, 2014, **2**, 14641.
5 C. Cheng, W. Ren and H. Zhang, *Nano Energy*, 2014, **5**, 132–138.
6 Z. Fang, Q. Wang, X. Wang, F. Fan, C. Wang and X. Zhang, *Mater. Res. Bull.*, 2013, **48**, 4935–4941.
7 X. Lai, J. E. Halpert and D. Wang, *Energy Environ. Sci.*, 2012, **5**, 5604.
8 D. Li, Q. Qin, X. Duan, J. Yang, W. Guo and W. Zheng, *ACS Appl. Mater. Interfaces*, 2013, **5**, 9095–9100.
9 L. Hu, H. Zhong, X. Zheng, Y. Huang, P. Zhang and Q. Chen, *Sci. Rep.*, 2012, **2**, 986.
10 L. Liu, Q. Fan, C. Sun, X. Gu, H. Li, F. Gao, Y. Chen and L. Dong, *J. Power Sources*, 2013, **221**, 141–148.
11 X. W. Lou, C. Yuan and L. A. Archer, *Adv. Mater.*, 2007, **19**, 3328–3332.
12 X. W. Lou and L. A. Archer, *Adv. Mater.*, 2008, **20**, 1853–1858.
13 A. Pan, H. B. Wu, L. Yu and X. W. Lou, *Angew. Chem., Int. Ed.*, 2013, **52**, 2226–2230.
14 C. Nethravathi, C. R. Rajamathi, M. Rajamathi, U. K. Gautam, X. Wang, D. Golberg and Y. Bando, *ACS Appl. Mater. Interfaces*, 2013, **5**, 2708–2714.
15 R. B. Rakhi, W. Chen, M. N. Hedhili, D. Cha and H. N. Alshareef, *ACS Appl. Mater. Interfaces*, 2014, **6**, 4196–4206.
16 C. Zhang, Z. Chen, Z. Guo and X. W. Lou, *Energy Environ. Sci.*, 2013, **6**, 974.
17 L. Huang, X. Zhao, L. Zhang, L. Y. Shi, J. P. Zhang and D. S. Zhang, *Nanoscale*, 2015, **7**, 2743–2749.
18 S. Cai, D. Zhang, L. Shi, J. Xu, L. Zhang, L. Huang, H. Li and J. Zhang, *Nanoscale*, 2014, **6**, 7346–7353.
19 J. Zhu, Z. Yin, D. Yang, T. Sun, H. Yu, H. E. Hoster, H. H. Hng, H. Zhang and Q. Yan, *Energy Environ. Sci.*, 2013, **6**, 987.
20 C. Niu, J. Meng, C. Han, K. Zhao, M. Yan and L. Mai, *Nano Lett.*, 2014, **14**, 2873–2878.
21 H. Li, D. Zhang, P. Maitarad, L. Shi, R. Gao, J. Zhang and W. Cao, *Chem. Commun.*, 2012, **48**, 10645–10647.
22 K. Kim do, P. Muralidharan, H. W. Lee, R. Ruffo, Y. Yang, C. K. Chan, H. Peng, R. A. Huggins and Y. Cui, *Nano Lett.*, 2008, **8**, 3948–3952.
23 S. Liang, T. Chen, A. Pan, D. Liu, Q. Zhu and G. Cao, *ACS Appl. Mater. Interfaces*, 2013, **5**, 11913–11917.
24 Y. Tang, D. Sun, H. Wang, X. Huang, H. Zhang, S. Liu and Y. Liu, *RSC Adv.*, 2014, **4**, 8328.
25 S. Liang, J. Zhou, G. Fang, X. Li, A. Pan, J. Wu, Y. Tang and J. Liu, *J. Alloys Compd.*, 2014, **583**, 351–356.
26 H. He, G. Jin, H. Wang, X. Huang, Z. Chen, D. Sun and Y. Tang, *J. Mater. Chem. A*, 2014, **2**, 3563.
27 H. Song, Y. Liu, C. Zhang, C. Liu and G. Cao, *J. Mater. Chem. A*, 2015, **3**, 3547–3558.
28 S. Huang, X. L. Wang, Y. Lu, X. M. Jian, X. Y. Zhao, H. Tang, J. B. Cai, C. D. Gu and J. P. Tu, *J. Alloys Compd.*, 2014, **584**, 41–46.
29 H. Wang, S. Liu, Y. Ren, W. Wang and A. Tang, *Energy Environ. Sci.*, 2012, **5**, 6173.
30 A. Q. Pan, H. B. Wu, L. Zhang and X. W. Lou, *Energy Environ. Sci.*, 2013, **6**, 1476.
31 Y. L. Ding, Y. Wen, C. Wu, P. A. van Aken, J. Maier and Y. Yu, *Nano Lett.*, 2015, **15**, 1388–1394.
32 S. H. Bae, S. Lee, H. Koo, L. Lin, B. H. Jo, C. Park and Z. L. Wang, *Adv. Mater.*, 2013, **25**, 5098–5103.
33 S. Liang, J. Zhou, G. Fang, J. Liu, Y. Tang, X. Li and A. Pan, *ACS Appl. Mater. Interfaces*, 2013, **5**, 8704–8709.
34 C. Wang, Z. Guo, W. Shen, Q. Xu, H. Liu and Y. Wang, *Adv. Funct. Mater.*, 2014, **24**, 5511–5521.
35 D. Sun, G. Jin, H. Wang, X. Huang, Y. Ren, J. Jiang, H. He and Y. Tang, *J. Mater. Chem. A*, 2014, **2**, 8009.
36 L. Liang, Y. Xu, Y. Lei and H. Liu, *Nanoscale*, 2014, **6**, 3536–3539.
37 C. Han, Y. Pi, Q. An, L. Mai, J. Xie, X. Xu, L. Xu, Y. Zhao, C. Niu, A. M. Khan and X. He, *Nano Lett.*, 2012, **12**, 4668–4673.
38 R. Baddour-Hadjean, S. Bach, N. Emery and J. P. Pereira-Ramos, *J. Mater. Chem.*, 2011, **21**, 11296.
39 S. Liang, J. Zhou, G. Fang, C. Zhang, J. Wu, Y. Tang and A. Pan, *Electrochim. Acta*, 2014, **130**, 119–126.

40 G. Nagaraju, S. Sarkar, J. Dupont and S. Sampath, *Solid State Ionics*, 2012, **227**, 30–38.
41 H. Liu, Y. Wang, L. Li, K. Wang, E. Hosono and H. Zhou, *J. Mater. Chem.*, 2009, **19**, 7885.
42 Y. Xu, X. Han, L. Zheng, W. Yan and Y. Xie, *J. Mater. Chem.*, 2011, **21**, 14466.
43 N. T. Hong Trang, N. Lingappan, I. Shakir and D. J. Kang, *J. Power Sources*, 2014, **251**, 237–242.
44 S. Liang, J. Zhou, X. Zhang, Y. Tang, G. Fang, T. Chen and X. Tan, *CrystEngComm*, 2013, **15**, 9869.
45 H. Wang, K. Huang, C. Huang, S. Liu, Y. Ren and X. Huang, *J. Power Sources*, 2011, **196**, 5645–5650.